Available online at www.sciencedirect.com

ScienceDirect

Procedia CIRP 41 (2016) 992 – 997

www.elsevier.com/locate/procedia

48th CIRP Conference on MANUFACTURING SYSTEMS - CIRP CMS 2015

FEM analysis of fiber laser welding of Titanium and Aluminum

Giuseppe Casalino[a], Michelangelo Mortello[a], Patrice Peyre[b]

[a] *Department of Mechanics, Mathematics and Management (DMMM), Politecnico di Bari, Viale Japigia 182, 70126 Bari, Italy*
[b] *Laboratoire de Procédés et Ingenierie en Mécanique et Matériaux (PIMMM), CNRS Arts et Métiers ParisTech, 151 Bd de l'Hôpital, 75013 Paris, France*

* Corresponding author. Tel.: 00390805962753; *.E-mail address:* giuseppe.casalino@poliba.it

Abstract

In this paper a simple and versatile model for simulating the laser welding process of lightweight metal sheets is presented. The study was aimed to predict, for assigned welding conditions, the seam morphology and to improve the comprehension of the main thermal aspects involved in the process. The programming was developed by using the Ansys parametric design language (APDL). The moving source was modelled by associating an internal heat generation to several specific elements in the weld zone. Both homogeneous and dissimilar joints were assembled in butt configuration. At first the model was used to simulate the homogeneous joining of 2 mm thick Ti6Al4V titanium alloy plates. Two different strategy of modeling were used for the observed fused zone geometries (V-shaped or X-shaped bead). Then, the fiber laser offset welding (FLOW) of dissimilar metal joints was assessed by modeling the assembly of 2 mm thick AA5754 aluminum alloy and T40 commercially pure titanium sheets. The calibration of the model was conducted by comparing temperature fields in the cross sections and thermal cycles at certain specific distances from the welding centerline. The accuracy of the model was demonstrated by the good agreement between experimental and numerical results.

Peer-review under responsibility of the scientific committee of 48th CIRP Conference on MANUFACTURING SYSTEMS - CIRP CMS 2015

Keywords: Titanium; Aluminum, Laser welding; Numerical simulation

1. Introduction

In the last years the demand for lightweight materials in aerospace and automotive industries has increased considerably. Since the reduction in weight of components and structures entails minor costs of production and fuel consumption, many researchers have investigated on customized lightweight materials and novel technologies [1]. Titanium alloys are employed for the realization of many components thanks to their properties, such as high strength-to-weight ratio, corrosion resistance, good fatigue behavior, and others [2]. On the other hand, aluminum alloy boast minor costs, lower density and sheet forming properties [3]. Laser welding is considered as one of the most useful methods to perform metal assemblies, because of the high versatility, high energy density in small spot dimension and high efficiency and productivity [4]. In particular, the high beam quality and the low wavelength made the fiber laser to ensure several advantages for welding metal materials. Absorptivity increases and the defectiveness gets reduced significantly thanks to the remarkable optical properties of the high brightness fiber sources [5].

Customized materials are currently employed for many applications, since they can be designed to present the optimal reaction (in terms of chemical, mechanical and thermal behavior) to specific severe working conditions. In particular dissimilar joints, which consist of assemblies made up of two different materials, have a great potential in numerous fields, thanks to the possibility to operate in spatially variable working conditions and the possibility to combine constructively the advantages of each single component. The assembly of dissimilar joints by the traditional methods are difficult mostly because of the formation of extended brittle intermetallic zones, mixing of phases, problems of mutual solubility and poor metallurgical compatibility.

Different studies have been conducted on laser welding processes of dissimilar joints [6-8]. In particular, the fiber laser offset welding (FLOW) is an innovative technique, which has demonstrated to be suitable for dissimilar welds [9, 10]. Figure 1 shows the application of this method to produce Al-Ti assemblies.

Peer-review under responsibility of the scientific committee of 48th CIRP Conference on MANUFACTURING SYSTEMS - CIRP CMS 2015
doi:10.1016/j.procir.2016.01.030

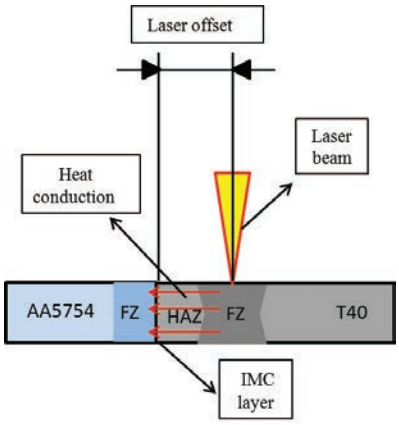

Fig. 1. Schematic representation of FLOW.

The beam was focused on the top surface of the Ti plate at a certain distance from the centerline, called offset. The keyhole formed in the Ti side and the heat is transferred from the keyhole to the interface because of convection and conduction phenomena. Although the temperatures at the interface are not sufficient to melt the Ti (heat-affected-zone formed) they lead to both the formation of a thin layer of intermetallic compounds (IMCs) and the diffusion of metal lamellae towards the Al side.
Nowadays, the optimization of manufacturing processes has aroused the interest of both industries and academic world for increasing productivity, reducing the number of experiments and full comprehending complex aspects involved in the processes. The capability of analytical methods is often unsuitable for finding desired solution within acceptable time and costs. Thus theoretical phenomena can be modelled by finite element method (FEM). This allows finding quantitative solutions by modeling the main aspects involved in each physical contribute.
The theoretical foundations for FEM simulating weld phenomena are described in Olabi's book chapter [11]. Although the simulation of welding processes is useful to manage heating and cooling phase, the task is challenging since it involves a multi-physical analysis for both fusion and solid state welding [12].
Many authors developed numerical model of welding processes. Zhang et al. investigated on the melting pool behavior and keyhole dynamics during full penetration laser welding [13].
Numerical simulation can be also used for predicting metallurgical transformation. This can be carried out by combining the temperature dependent material properties and the continuous cooling transformation diagrams [14]. Kazemi et al. demonstrated numerically, which are the most sensitive parameters that influence the bead shape [15]. Many authors determined the temperature distribution in the seam with the aim to predict the geometry of the bead for various welding conditions [16, 17].
Different strategies for modeling the thermal source were used [18]. Also laser welding of dissimilar joints was modelled by some authors. For example Chen et al. studied the interfacial reaction non-homogeneity by supporting the experiments with a FEM model [19].
In this work, the thermal behavior of fiber laser autogenously welded Ti6Al4V joints and AA5754-T40 dissimilar joints in butt configuration was simulated by FEM analysis. Different welding conditions and seam morphologies were modelled. Temperature fields and thermal cycles were analyzed for calibration. The model developed resulted to be versatile, simple and accurate.

2. Numerical procedure

2.1 Laser welding of Ti6Al4V

Ti6Al4V titanium alloy plates with a thickness of 2 mm were autogenously laser welded. The fiber laser beam was focused on the top surface of the work-piece along the interface centerline.
Two different combinations of process parameters were assessed (see Tab.1) with the aim to investigate on two different bead shapes (V-shaped bead and X-shaped bead). Linear energy is the ratio of the power to the welding speed and it indicates the amount of energy input transmitted to the work-piece.
The formation of an X-bead bead is favored by high energy input, whereas the formation of a V-shaped bead is favored by lower energy input.

Table 1. Process parameters adopted.

Sample	Laser Power (kW)	Welding Speed (m/min)	Linear energy (J/mm)	Expected bead shape
1	1.20	1.00	72.00	V
2	1.20	2.50	28.80	X

Ansys commercial code was used by adopting the parametric design language (APDL). This last is a scripting language used to automate common tasks, build parametric models, create constructs, solve algebraic operation with matrix and vectors, and other functions. The geometry of the plates (width x length x thickness) was 200x100x2 mm.
The following assumptions were made:

- The physical properties of the material at the solid state were assumed isotropic and temperature-dependent according to data found in the metal handbook. On the other hand, the properties at the molten state were estimated on the basis of the experimental observation, during the validation step.
- Irradiation, convective melt flows, keyhole dynamics, viscous forces and buoyancy forces were considered negligible.
- The continuity condition was imposed at the contact interface between the sheets.
- Energy losses caused by slow air convection at the upper and lateral surfaces were fixed at 20 W/m^2K. The thermal exchange between the work-piece and the support was taken into account by adopting a convective coefficient of 200 W/m^2K.
- The starting temperature was assumed equal to 20 °C.

As indicated in figure 2, a finer mesh was adopted in proximity to the welding centerline.

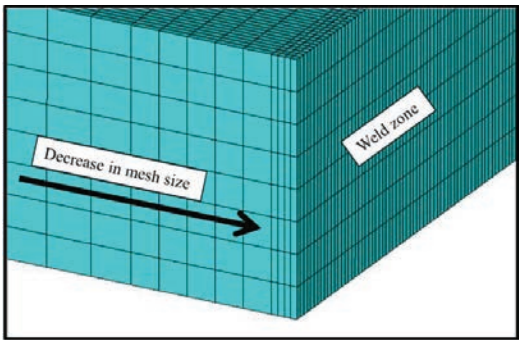

Fig. 2. Meshing of the sheet: interface close-up.

The partial differential equation 1 expresses the thermal balance per unit of volume of three contributes, i.e. transient heat conduction, heat input and increase in thermal energy.

$$\left\{k(T)\left(\frac{\partial^2 T}{\partial x^2}\right)+\left(\frac{\partial^2 T}{\partial y^2}\right)+\left(\frac{\partial^2 T}{\partial z^2}\right)\right\}+\dot{Q}=\rho(T)C_p(T)\frac{\partial T}{\partial t} \quad (1)$$

A simple method was adopted to simulate the power transmitted by the source during the welding. Since the process was simulated in keyhole regime, an internal production of heat was associated to several specific elements. Thus, the analysis was carried out by using an eight-node quadratic 3D solid element SOLID 70, which degree of freedom was the only temperature. Various convergences tests were conducted to find a suitable number of elements to discretize the whole geometry. The purpose was clearly to achieve a reasonable compromise between time for computing and accuracy. The heat generation rate HG was input as element body load at the nodes. It is expressed by the equation 2, as the ratio of the total power transmitted by the laser source to the total volume of the bead. This last consisted of the sum of the volumes of the elements selected for the application of the heat generation.

$$HG = Ptot/V \quad (2)$$

Two different welding cases were analysed, depending on the expected seam geometry:

- The case 1 was typical of a V-shaped bead. For the application of the heat generation HG the nodes were selected in a spherical local system. The selection is shown in figure 3.
- The case 2 was typical of an X-shaped bead. The nodes were selected in a double spherical local system. The selection is shown in figure 4.

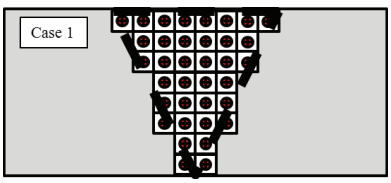

Fig. 3. Node selection for a V-shaped bead.

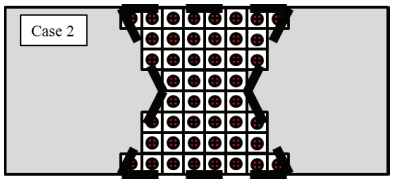

Fig. 4. Node selection for an X-shaped bead.

The history of the nodal temperature during the time for processing was calculated. The time evolution was simulated by adopting a DO loop cycle. A mobile coordinate system was imposed along the welding centerline. The coordinate along the welding direction was increased for each step by an amount equal to the radius of the beam. The thermal load distribution was computed at the beginning of each cycle of the loop. The time required for each step resulted from the ratio between the linear extension of the step and welding speed. The model validation was conducted by comparing both the cross sections and the thermal cycles. The morphology of the experimental bead, which mostly derived from the peak temperatures reached during the welding, was compared with the temperature fields calculated numerically. Thermocouples were positioned 2 mm far from the welding centerline. Thus the numerical and experimental thermal cycles were analyzed. After comparing the numerically computed solutions with the experimental obsverations , a coefficient K_{cal} was introduced to calibrate the model through the correction of the value of HG into HG_{corr} (see equation 3).

$$HG_{corr} = HG * K_{cal} \quad (3)$$

2.2 Laser offset dissimilar welding of T40 and AA5754

T40 commercially pure titanium and AA5754 aluminum alloy plates were welded by adopting the FLOW technique. As concerns the main numerical aspects (definition of geometry, meshing, hypotheses, boundary conditions, strategy of modeling of the moving source) the same assumption mentioned for the welding of the Ti6Al4V plates were made. Since in previous studies the condition of X-shaped bead was considered favorable in terms of quality of the seams, the case 2 (see figures 3 and 4) was chosen for simulating the FLOW of the dissimilar joints. However, unlike the homogenous welding of the Ti6Al4V plates a more detailed analysis was conducted on the contact interface between the sheets. During the FLOW technique the roughness of contact interface and the heat conduction are very relevant for the diffusion of chemical species through the interface layer (necessary for dissimilar joining). Since the heat conduction involved the only contact zones the thermal resistance in the gap between the sheets result to influence significantly the formation of the seam. Thus, an interface layer, which simulates the thermal coupling, was positioned between the plates. As shown in figure 5, as concerns the contact pair, 3D surface-to-surface contact elements CONTA174 and target element TARGE170 were adopted to mesh the interface layer. These elements were selected to consider the large deflection and nonlinear behavior of contact asperities. The conductive heat transfer between two contacting surfaces is defined by the thermal conductance contact (TTC).

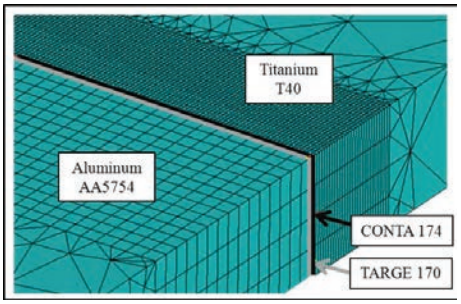

Fig. 5. Meshing at the proximity of the interface for dissimilar weld.

The equation 4 expresses the thermal flow for a unity of contact area (Q cont).

$$Q_{cont} = TTC * (T_T - T_C) \quad (4)$$

(T_T-T_C) is the difference between the temperatures of the contact elements (TARGE170 and CONTA174).

3. Results

3.1 Validated model for Ti6Al4V joints

Figures 6 and 7 show the comparison between experimental and numerical results for both the welding conditions assessed (i.e. V-shaped bead and X-shaped bead respectively). The legend of the temperature ranges is indicated on the right side of each picture.. After validating the model, the results achieved were satisfactory. In fact, numerical temperature fields approached the morphology of the seam with a good accuracy.

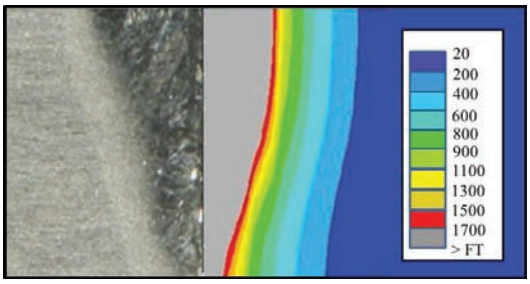

Fig. 6. Comparison of cross sections for a V-shaped bead.

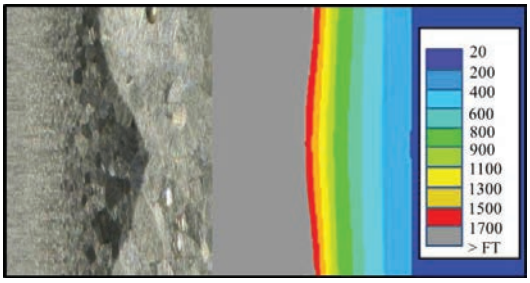

Fig. 7. Comparison of cross sections for an X-shaped bead.

3.2 Validated model for T40-AA5754 dissimilar joints

Figure 8 shows the position of thermocouples adopted for validating the model. They were positioned on both the sides at distances of 2 and 3 mm from the interface.
The experimental and numerical thermal cycles are shown in figures 9 and 10, respectively, referring to the zones indicated in figure 8. The numerical curves approached the experimental ones. In fact, the analysis of the computed curves has shown that the main features of the curves are much closed to each other (peak temperatures, heating and cooling rates, etc.).
A slight disagreement was caused by the assumptions made during the phase of definition of material properties, boundary conditions and modeling of thermal source. However, those made the model simple and efficient in terms of accuracy and time for computing.

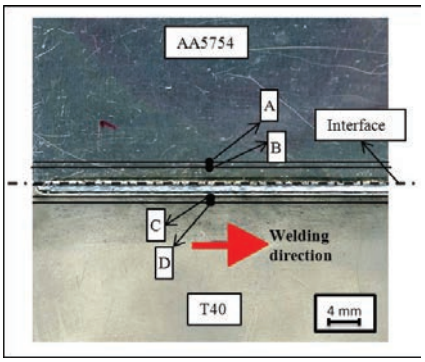

Fig. 8. Position of thermocouples for dissimilar weld.

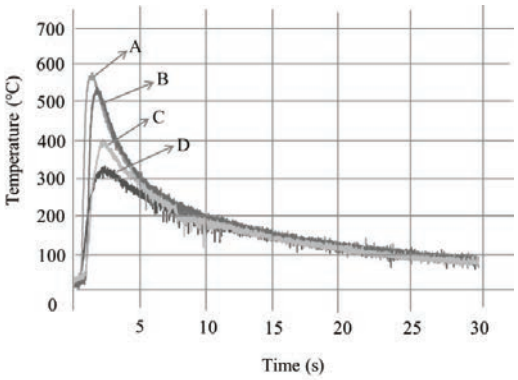

Fig. 9. Experimental thermal cycles for the dissimilar weld.

At first, the analysis of temperatures in the proximity of the contact interface was carried out without using an interface layer, which simulates the behavior of the thermal pair. However, in this way, the numerical results were not compatible with the experimental observations.
Figures 11 and 12 show the solutions found by adopting the contact elements (TARGE170 and CONTA174).
Figure indicates the temperature range. Temperature profile at the mid thickness was computed by the numerical model, whose results are shown in figure 11.

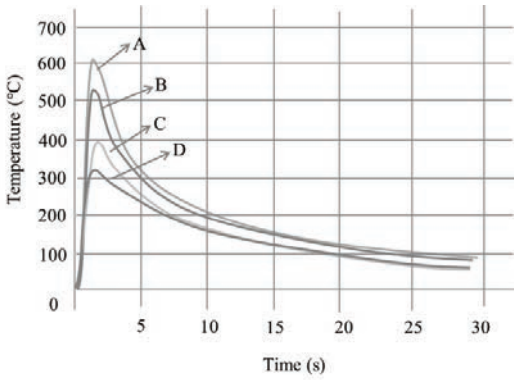

Fig. 10. Numerical thermal cycles for the dissimilar weld.

A slight asymmetry of the temperature fields about the mid thickness was due to the assumptions made about the thermal exchange, which occurred at the top and bottom side of the work-piece. On the other hand, figure 12 shows the temperature fields at the top surface when the laser source has completed the 75% of its path.

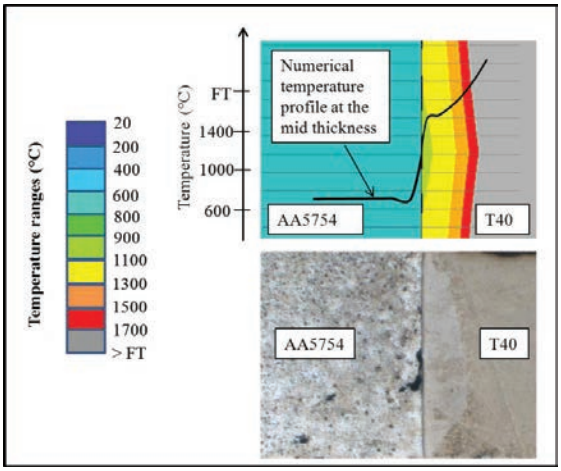

Fig. 11. Comparison of temperature fields for the dissimilar weld.

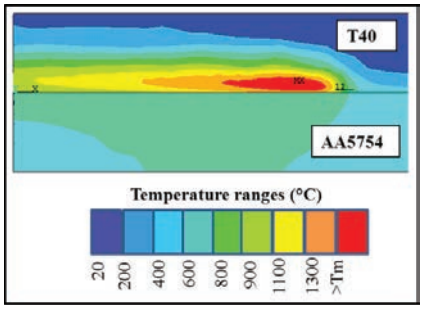

Fig. 12. Temperature fields at the top surface of the work-piece.

As described by the picture the source determined a quasi-elliptical temperature distribution. The large difference in thermos-physical properties and the action of the contact elements promoted a gap between the thermal behaviors of the sheets.

4. Conclusions

In this work, the thermal simulation of fiber laser autogenous welding of Ti6Al4V joints and AA5754-T40 joints in butt configuration was simulated by FEM analysis. The following conclusions are reported.

- The model developed resulted to account for complex phenomena arising during the laser welding into a simple and versatile numerical scheme.
- Depending on the expected seam shape various welding conditions the process can be re-produced by varying the thermal load and the node selection.
- A good agreement between experimental and numerical results was demonstrated by the comparison of temperatures and thermal cycles.
- The thermal behavior at the contact interface was simulated efficiently, as confirmed by the comparison of numerical and experimental temperature fields in the weld zone.
- The model resulted capable to predict the thermal behavior of metal joints performed by both traditional laser welding and FLOW method.

References

[1] Martinse K., Hu S.J., Carlson, B.E. Joining of dissimilar materials. CIRP Annals 2015; 64:679-699.
[2] Veiga C, Davim J P, Loureiro A J R. Properties and applications of titanium alloys: a brief review. ADV. Mater. Sci. 2012; 32:133-148.
[3] Miller W S, Zhuang a L, Bottema J, Wittebrood A J, De Smet P, Haszler A, Vieregge A. Recent development in aluminium alloys for the automotive industry. Materials Science and Engineering 2000; A280; 37–49.
[4] Casalino, G., Mortello, M., Leo, P., Benyounis, K.Y., Olabi, A.G. Study on arc and laser powers in the hybrid welding of AA5754 Al-alloy. Materials and Design 2014, 61, 191-198.
[5] Quintino L, Costa A, Miranda R, Yapp D, Kumar V, Kong C J. Welding with high power fiber lasers – A preliminary study. Materials and design 2007; 28, No. 4: 1231-1237.
[6] Casalino, G., Campanelli, S.L., Ludovico, A.D. Laser-arc hybrid welding of wrought to selective laser molten stainless steel. Int. J. of Adv. Man. Tech. 2013, 68, 1-4, 209-216.
[7] Chen S, Li L, Chen Y, Huanga J. Joining mechanism of Ti/Al dissimilar alloys during laser welding-brazing process. Journal of Alloys and Compounds 2011; A509; 891–898.
[8] Chengwu Yao, BinshiXu, XianchengZhang, JianHuang, JunFu, YixiongWu. Interface microstructure and mechanical properties of laser welding copper–steel dissimilar joint. Optics and Lasers in Engineering 2009; 47: 807–814.
[9] Casalino G, Mortello M, Peyre P. Yb-YAG laser offset welding of AA5754 and T40 butt joint. Journal of materials processing technology 2015; 223: 139-149.
[10] Casalino G,Mortello M. Modeling and experimental analysis of fiber laser offset welding of Al-Ti butt joints. International Journal of Advanced Manufacturing Technology 2015; DOI: 10.1007/s00170-015-7562-8.
[11] Olabi A G, Casalino G. Mathematical Modeling of weld phenomena, part I: Finite-element modeling. Comprehensive Materials Processing 2014; 214, 6:101-109.
[12] Casalino, G., Contuzzi, N., Minutolo, F.M.C., Mortello, M. Finite element model for laser welding of titanium. Procedia CIRP 2015, 33, 434-439.
[13] Zhang L J, Zhang J X, Gumenyuk A, Rethmeier M, Na S J. Numerical simulation of full penetration laser welding of thick steel plate with high power high brightness laser. Journal of materials processing technology 2014; 214: 1710-1720.
[14] Tsrikas S A, Papanikos P, Kermanidis Th. Numerical simulation of the laser welding process in butt-joints specimens. Journal of materials processing

technology 2003; 134: 59-69.
[15] Kazemi L, Goldak J A. Numerical simulation of laser full penetration welding. Computational Materials Science 2009; 44: 841-849.
[16] Hanbin Du, Lunji Hu, Jianhua Liu, Xiyuan Hu. A study on the metal flow in full penetration laser beam welding for titanium alloy. Computational Materials Science 2004; 29: 419–427.
[17] Akbari M, Saedodin S, Toghraie D, Shoja-Razavi R, Kowsari F. Experimental and numerical investigation of temperature distribution and melt pool geometry during pulsed laser welding of Ti6Al4V alloy. Optics and laser technology 2014; 59: 52-59.
[18] Mackwood A P, Craferb R C. Thermal modelling of laser welding and related processes: a literature review. Optics & Laser Technology 2005; 37: 99–115.
[19] Chen S, Li L, Chen Y, Huanga J. Joining mechanism of Ti/Al dissimilar alloys during laser welding-brazing process. Journal of Alloys and Compounds 2011; A509; 891–898.